

Exact fixed-point tensor network construction for rational conformal field theory

Gong Cheng,^{1,2,*} Lin Chen,^{3,*} Zheng-Cheng Gu,^{4,†} and Ling-Yan Hung^{5,‡}

¹Department of Physics, Virginia Tech, Blacksburg, VA 24060, USA

²Maryland Center for Fundamental Physics, University of Maryland, College Park, MD 20740, USA

³School of Physics and Optoelectronics, South China University of Technology, Guangzhou 510641, China

⁴Department of Physics, The Chinese University of Hong Kong, Shatin, New Territories, Hong Kong, China

⁵Yau Mathematical Sciences Center, Tsinghua University, Haidian, Beijing 100084, China

(Dated: May 17, 2024)

The novel concept of entanglement renormalization and its corresponding tensor network renormalization technique have been highly successful in developing a controlled real space renormalization group (RG) scheme. Numerically approximate fixed-point (FP) tensors are widely used to extract the conformal data of the underlying conformal field theory (CFT) describing critical phenomena. In this paper, we present an explicit analytical construction of the FP tensor for 2D rational CFT. We define it as a correlation function between the "boundary-changing operators" on triangles. Our construction fully captures all the real-space RG conditions. We also provide a concrete example using the Ising model to compute the scaling dimensions explicitly based on the corresponding FP tensor. Interestingly, our construction of FP tensors is closely related to a strange correlator, where the holographic picture naturally emerges. Our results also open a new door towards understanding CFT in higher dimensions.

Introduction — In the past two decades, the novel concept of entanglement renormalization [1–5] has been developed to study critical systems. In particular, computationally efficient algorithms has been proposed based on tensor network techniques, such as various schemes of tensor network renormalization (TNR) [2, 5–10]. It is found that even with a moderate size of bond dimensions kept in the coarse graining procedure, there are lots of important information such as central charge, scaling dimensions and operator product expansion(OPE) coefficient of conformal field theory(CFT) can be read off from the fixed point (FP) tensors, which are approximate fixed points of the TNR algorithms [5, 10]. Despite the huge successes in numerically extracting conformal data through tensor network simulations, the analytical construction of FP tensors for critical systems remains a significant challenge. While progress has been made in understanding the components of FP tensors associated with primary fields [11, 12], generalizing these constructions for descendant fields remains unclear. On the other hand, the recently proposed holographic picture and generalized symmetry description [13–15] for CFT suggest that the complete algebraic structure of FP tensors might provide us an alternative way to understand CFT, which will lead to a revolution in modern physics.

In this paper, we demonstrate that the collection of open string correlation functions conformally related to an open pair of pants in every rational CFT (RCFT) yields an exact infinite-dimensional FP tensor. By tiling these correlators over a given manifold and summing over all intermediate states, including primaries and descendants, we obtain the RCFT path integral. However, this tiling process leaves behind holes, which must be reconciled for the correlators to match with an FP tensor. Previous research [16] introduced shrinkable boundary con-

ditions that address this problem and was further studied in [17]. By combining these boundary conditions with the open correlators, we achieve a field theoretical construction of tensors that satisfy the expected properties of a FP tensor. To validate our approach, we provide explicit numerical examples, focusing on the Ising model. Our results demonstrate convincingly that our proposed FP tensors can accurately recover the closed spectrum of the exact CFT when tiling a cylinder.

Finally, we stress that our construction of FP tensors coincides with constructing an eigenstate $\langle \Omega |$ of the topological RG operator associated to a fusion category \mathcal{C} [18, 19], and expressing the CFT partition function as a *strange correlator* [20], namely $Z_{CFT} = \langle \Omega | \Psi \rangle$, where $|\Psi\rangle$ is the ground state wave-function of the Levin-Wen model [21], or Turaev-Viro topological quantum field theory (TQFT) [22], associated also to category \mathcal{C} [23].

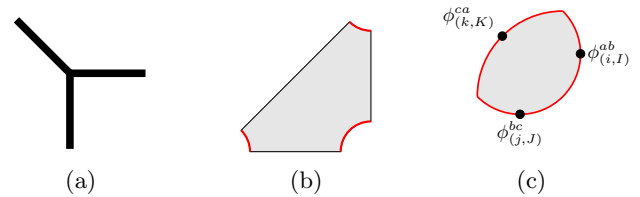


FIG. 1: (a) denotes the rank-3 tensor, corresponds to a path integral over the shaded region (b). (c) denotes correlation function of three local operators on a disk with conformal boundary condition on the red edge.

The structure of FP Tensor — The FP tensor we propose, denoted as $\mathcal{T}_{(i,I)(j,J)(k,K)}^{abc}$, comprises nine indices. The labels a, b, c correspond to the conformal boundary conditions of the RCFT, while i, j, k represent the labels of the RCFT primaries, and the indices I, J, K pertain

to the descendants of their respective primaries. In the RCFT, a, b, c and i, j, k take values from a finite set, while I, J, K live in an infinite-dimensional space. Consequently, the exact FP tensors possess an infinite bond dimension, as expected. The FP tensor, $\mathcal{T}_{(i,I)(j,J)(k,K)}^{abc}$, can be interpreted as the path integral of the CFT within an open triangle. To regulate the path integral, we slightly modify the corners of the triangle and impose conformal boundary conditions labeled as a, b , and c at each respective corner. The edges of the triangle correspond to states that represent boundary-changing operators that connect the two conformal boundaries associated with the given edge.

To show that they correspond to FP tensors, we need to demonstrate two properties: (a) the FP tensors should satisfy crossing relations; (b) FP tensors covering a large patch upon contraction reproduce exactly the same FP tensors covering a smaller patch; (c) Tiling the FP tensors on a surface and assigning appropriate contraction of the indices recover the CFT path-integral on the surface. These conditions are illustrated in Fig. 3 and Fig. 4. As we will see, these requirements ensure that the FP tensors reconstruct the CFT partition function exactly.

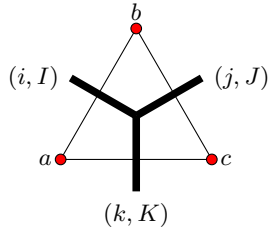


FIG. 2: Diagrammatic representation of the tensor. The base triangle denotes the structure coefficient C_{ijk}^{abc} , and the rank-3 tensor on top of it denotes the conformal block α_{IJK}^{ijk} which carries descendants information.

In general, the FP tensor can be decomposed as:

$$\mathcal{T}_{(i,I)(j,J)(k,K)}^{abc} = \alpha_{IJK}^{ijk} C_{ijk}^{abc} \quad (1)$$

This is because a three-point correlation function of three boundary operators carries two parts, represented diagrammatically in Fig. 2, namely the structure coefficients C_{ijk}^{abc} and the conformal blocks carrying the dependence of the correlation function on the precise descendent in the primary families, the location of insertions, and the precise shape of the manifold in which operators are inserted. To set our notations, the three point correlation functions of three primary boundary changing operators

on the upper-half plane is given by:

$$\langle \phi_{(i,0)}^{ab}(x_1) \phi_{(j,0)}^{bc}(x_2) \phi_{(k,0)}^{bc}(x_3) \rangle = C_{ijk}^{abc} \beta_{000}^{ijk}(x_1, x_2, x_3), \quad (2)$$

$$\beta_{000}^{ijk}(x_1, x_2, x_3) = \frac{1}{|x_1 - x_2|^{\Delta_i + \Delta_j - \Delta_k} |x_1 - x_3|^{\Delta_i + \Delta_k - \Delta_j} |x_3 - x_2|^{\Delta_k + \Delta_j - \Delta_i}}, \quad (3)$$

where $I = J = K = 0$ denotes the fact that the inserted operators are all primaries. Conformal blocks involving other descendants where $I, J, K \neq 0$ can be generated by repeated use of the Virasoro or generally Kac-Moody operators in the primaries.

In our proposed FP tensor, $\alpha_{IJK}^{ijk} = \chi \circ \beta_{IJK}^{ijk}$, where $x_{1,2,3}$ are fixed and suppressed in the following, and χ denotes a conformal map from the upper half plane to a triangle. This map is detailed in the Supplemental Material. These α_{IJK}^{ijk} satisfies:

$$\sum_M \alpha_{IJM}^{ijm} \alpha_{MKL}^{mkl} = \sum_{n,N} [F_l^{ijk}]_{mn}^{\text{blocks}} \alpha_{INL}^{inl} \alpha_{JKN}^{jkn}, \quad (4)$$

where $[F_l^{ijk}]_{mn}^{\text{blocks}}$ are the crossing coefficients characterising this RCFT. The same matrix F^{blocks} also relate structure coefficients C_{ijk}^{abc} through the equation,

$$\sum_m [F_l^{ijk}]_{mn}^{\text{blocks}} C_{ijm}^{abc} C_{mkl}^{acd} = C_{inl}^{abd} C_{jkn}^{bcd}. \quad (5)$$

This guarantees the proposed FP tensor satisfies the crossing relation in condition (a).

$$\begin{aligned} & \sum_{m,M} \mathcal{T}_{(i,I)(j,J)(m,M)}^{abc} \mathcal{T}_{(m,M)(k,K)(l,L)}^{acd} \\ &= \sum_{n,N} \mathcal{T}_{(i,I)(n,N)(l,L)}^{abd} \mathcal{T}_{(j,J)(k,K)(n,N)}^{bcd}. \end{aligned} \quad (6)$$

Diagrammatically, this is illustrated in Fig. 3, which follows from the crossing symmetry of the RCFT.

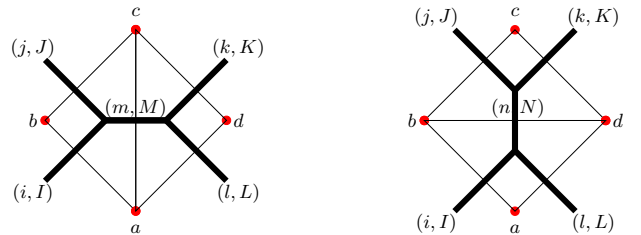


FIG. 3: crossing symmetry

The FP tensor also satisfies the coarse graining condition (b), which is illustrated in Fig. 4.

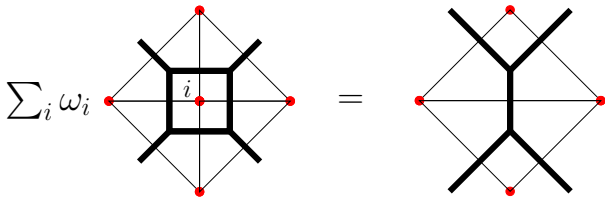


FIG. 4: coarse graining

We note that the vertex degree of freedom at the center is summed over with a weight w_i . For a diagonal RCFT,

$$w_i = S_{00}^{1/2} S_{i0}, \quad (7)$$

Physically, the coarse-graining condition implies that when we sew the four triangles by contracting the shared descendant labels between neighboring triangles, a small hole is left in the middle. This hole disappears when we sum over the conformal boundary conditions with weights given by (7). The idea of this weighted sum of conformal boundary conditions was initially explored in [16] within the context of entanglement brane boundary conditions. It suggests that the boundaries arising in the computation of the entanglement entropy are artificial and should be "contractible." These considerations motivated the use of this particular weighted sum.

The open boundary can be transformed through a modular transformation into a closed conformal boundary Cardy state $|i\rangle_c$. It can be shown that the weighted sum of the boundaries yields:

$$\sum_i \omega_i |i\rangle_c = |0\rangle, \quad (8)$$

where the right-hand side corresponds to the identity of the Ishibashi state. When the hole is small, the dominant contribution arises from the leading term, which is the vacuum state. The leading corrections then come from the leading descendant of the vacuum state, which can be viewed as an irrelevant perturbation in the thermodynamic limit of the tiling, as explained in [17]. This boundary conditions are physical reasons behind condition (b) and (c) satisfied by the FP tensor.

The partition function of the CFT on a manifold M can be obtained using the following procedure. We begin by triangulating the manifold M into a collection of triangles Δ . Each edge e on a triangle is labeled with a pair of primary and descendant labels (i, I) , and each vertex v is labeled with a conformal boundary condition a . On each triangle, we assign a tensor $\mathcal{T}_{(i,I)(j,J)(k,K)}^{abc}$ based on the labeling of the edges and vertices. The proposed partition function is then given by:

$$Z_M = \sum_{\{(i,I)\}, \{a\}} \prod_v \omega_a \prod_{\Delta} \mathcal{T}_{(i,I)(j,J)(k,K)}^{abc}. \quad (9)$$

A simple example: the Ising CFT — In the Ising example, we can put in explicit expressions to the above

construction. The closed Ising CFT has three primaries $\mathcal{C}_{Is} = \{I, \sigma, \psi\}$. The theory has three conformal boundary conditions. They are labeled as $\{+, -, f\}$, corresponding to the respective primaries. The Hilbert space for an interval with left and right boundary given by a and b respectively, where $a, b \in \mathcal{C}_{Is}$ is given by $\mathcal{H}_{ab} = \oplus_c N_{ab}^c V_c$, where V_c is the space corresponding to the primary representation labeled $a \in \mathcal{C}_{Is}$, and $N_{ab}^c \in \mathbb{Z}_{\geq 0}$ are the fusion coefficient among the objects \mathcal{C}_{Is} , with: $N_{Ib}^c = \delta_{bc}$, $N_{\sigma\sigma}^c = 1 - \delta_{c\sigma}$, $N_{\sigma a \neq \sigma}^b = \delta_{b\sigma}$, $N_{\psi\psi}^b = \delta_{bI}$.

The matrix $[F_l^{ijk}]^{\text{blocks}}$ is provided in Supplemental Material. Using Eq. (5), we calculate the structure coefficients C_{ijk}^{abc} . Below we list those values other than 1:

$$\begin{aligned} C_{III}^{\pm\pm\pm} &= C_{\psi\psi I}^{\pm\mp\pm} = C_{\sigma\sigma I}^{\pm f\pm} = 2^{\frac{1}{4}}, \\ C_{\sigma\sigma\psi}^{\pm f\mp} &= \frac{1}{2^{\frac{1}{4}}}, C_{\sigma\sigma\psi}^{f+f} = \frac{1}{\sqrt{2}}, C_{\sigma\sigma\psi}^{f-f} = -\frac{1}{\sqrt{2}} \end{aligned} \quad (10)$$

We have to compute the three point functions involving descendants, and then transform them into the needed geometry using the conformal map that is relegated to the Supplemental Material. Explicitly, one has to look for the orthogonal basis of the descendants. For example, in level one, the normalized first descendant $O^{(-1)}$ is defined as $\frac{1}{\sqrt{2\Delta}} L_{-1} O$. It's transformation under the conformal map $\chi(z)$ is:

$$\chi_*[O^{(-1)}] = |\chi'(0)|^\Delta \left(\chi'(0) O^{(-1)} + \sqrt{\frac{\Delta}{2}} \frac{\chi''(0)}{\chi'(0)} O \right). \quad (11)$$

In the second level, we find three normalized operators.

$$\mathbb{1}^{(-2)} = 2L_{-2}\mathbb{1}, \quad (12)$$

$$\psi^{(-2)} = \frac{6}{25} L_{-2}\psi + \frac{9}{25} L_{-1}^2\psi, \quad (13)$$

$$\sigma^{(-2)} = \frac{16\sqrt{2}}{25} L_{-2}\sigma + \frac{12\sqrt{2}}{25} L_{-1}^2\sigma. \quad (14)$$

and the corresponding transformation rules given by:

$$\begin{aligned} \chi_*[L_{-2}O] &= (\chi')^2 L_{-2}O + \frac{3}{2} \chi'' L_{-1}O + \\ &\left(\frac{c\chi'''}{12\chi'} - \frac{c(\chi'')^2}{8(\chi')^2} + \frac{2\chi'''\Delta}{3\chi'} - \frac{(\chi'')^2\Delta}{4(\chi')^2} \right) O, \end{aligned} \quad (15)$$

$$\begin{aligned} \chi_*[L_{-1}^2O] &= (\chi')^2 L_{-1}^2O + (2\Delta + 1)\chi'' L_{-1}O + \\ &\left(\frac{\chi'''\Delta}{\chi'} + \frac{(\chi'')^2\Delta(\Delta - 1)}{(\chi')^2} \right) O. \end{aligned} \quad (16)$$

For higher level descendants, we derive iteration equations to solve all the transformation rules. Additionally, the three-point correlation functions for descendant fields are also calculable by iteration methods. The details are also illustrated in the Supplemental Material. We checked crossing relations 1) and 2), keeping only three descendants in each conformal family. Despite the very

small bond dimension, we find that they are satisfied to an accuracy of 2×10^{-3} .

Considering the example of fixing the four external legs as $(\mathbb{1}, \mathbb{1}, \mathbb{1}, \mathbb{1})$ and the four boundary conditions to be $(+, +, +, +)$, we compute the following contraction:

$$T_{L.H.S.} := [(T_{\mathbb{1}\mathbb{1}\mathbb{1}}^{+++})^4 + (T_{\psi\psi\mathbb{1}}^{+-+})^4 + \sqrt{2}(T_{\sigma\sigma\mathbb{1}}^{+f+})^4]/2\sqrt{2}. \quad (17)$$

where we didn't write the descendant field indices and they are understood as being contracted implicitly. Similarly contracting two tensors we get

$$T_{R.H.S.} = (T_{\mathbb{1}\mathbb{1}\mathbb{1}}^{+++})^2. \quad (18)$$

Finally, We demonstrate that our proposed FP tensor constructed from open correlation functions can indeed recover the closed spectrum with surprisingly high accuracy despite keeping only very few descendants in each family. The cylinder is constructed using 4 squares formed out of 8 triangles, as shown in Supplemental Material. The labels of the conformal boundaries at the top and the bottom edge of the cylinders are treated alongside the primaries and descendent labels of the FP tensors as input and output indices of the cylinder. One can solve for the spectrum of the cylinder, which is listed in the Table I below. In the Supplemental Material we provide details on how the numerical conformal dimension converges towards the precise value as we increase the cutoff in descendant level.

States	Numerical dim	Accurate dim
$\mathbb{1}$	0.0000	0.0000
σ	0.1250	0.1250
ϵ	0.9989	1.0000
$\partial\sigma, \bar{\partial}\sigma$	1.1253	1.1250
$\partial\epsilon, \bar{\partial}\epsilon$	2.0004	2.0000
$\mathbb{1}^{(-2)}, \bar{\mathbb{1}}^{(-2)}$	1.9986	2.0000
$\partial\bar{\partial}\sigma$	2.1099	2.1250
$\sigma^{(-2)}, \bar{\sigma}^{(-2)}$	2.1208	2.1250
$\partial\bar{\partial}\epsilon$	2.9517	3.0000
$\partial^2\epsilon, \bar{\partial}^2\epsilon$	3.0030	3.0000
$\mathbb{1}^{(-3)}, \bar{\mathbb{1}}^{(-3)}$	2.9496	3.0000
$\bar{\partial}\sigma^{(-2)}, \partial\bar{\sigma}^{(-2)}$	2.9900	3.1250
$\partial\sigma^{(-2)}, \bar{\partial}\bar{\sigma}^{(-2)}$	3.1167	3.1250
$\sigma^{(-3)}, \bar{\sigma}^{(-3)}$	3.1291	3.1250
$\mathbb{1}^{(-2, -\bar{2})}$	4.0323	4.0000

TABLE I: Conformal dimensions obtained by diagonalizing the transfer matrix, compared with the accurate data.

FP tensors as eigenstates of topological RG operators — While the FP tensor can be understood directly as a CFT correlation function without explicit reference to an associated 3d TQFT, it is an important observation that

these FP tensors follows from an exact eigenstate of the topological RG operator [18, 24], and the CFT partition function can be written explicitly as a *strange correlator*.

To appreciate this connection, recall that the label set of primaries in an RCFT are objects in a modular fusion category \mathcal{C} . Here we focus on diagonal RCFT so that the conformal boundary conditions are also labeled by objects in \mathcal{C} . It is convenient to re-scale the three point conformal block $\alpha_{IJK}^{ijk} = \mathcal{N}_{ijk} \gamma_{IJK}^{ijk}$, where [25],

$$\mathcal{N}_{ijk} = \sqrt{\theta(i, j, k) / \sqrt{d_i d_j d_k}}, \quad (19)$$

where $\theta(i, j, k) = d_i / [F^{jkkj}]_{\mathbb{1}_i}^{\text{blocks}}$, and d_i is the quantum dimension of object i , which is related to the modular matrix by $d_i = S_{0i}/S_{00}$ for a diagonal RCFT. The value of the FP tensor (1) does not change, except that it is decomposed instead as $\mathcal{T}_{(i,I)(j,J)(k,K)}^{abc} = \gamma_{IJK}^{ijk} \hat{C}_{ijk}^{abc}$. On this basis, the structure coefficients \hat{C}_{ijk}^{abc} of a diagonal RCFT (including the Ising CFT described above) can be written simply as [26],

$$\hat{C}_{ijk}^{abc} = (d_i d_j d_k)^{1/4} \left[\begin{array}{ccc} i & j & k \\ c & a & b \end{array} \right], \quad (20)$$

where the square bracket denotes the quantum 6j-symbols of the modular tensor category \mathcal{C} associated to the RCFT in with tetrahedral symmetry and chosen normalization. Several components in this gauge involving the identity label are fixed to the values reviewed in the Supplemental Material. All two point correlations are also normalised. These γ_{IJK}^{ijk} inherit the crossing relation of (4), with the crossing kernel re-scaled as:

$$[F_l^{ijk}]_{mn} = [F_l^{ijk}]_{mn}^{\text{blocks}} \frac{\mathcal{N}_{jkn} \mathcal{N}_{inl}}{\mathcal{N}_{ijm} \mathcal{N}_{mkl}}. \quad (21)$$

These re-scaled crossing kernels $[F_l^{ijk}]_{mn}$ is related to the quantum 6j-symbol above by:

$$[F_l^{ijk}]_{mn} = \sqrt{d_m d_n} \left[\begin{array}{ccc} i & j & m \\ k & l & n \end{array} \right]. \quad (22)$$

The explicit values of $[F_l^{ijk}]_{mn}$ and $[F_l^{ijk}]_{mn}^{\text{block}}$ for the Ising CFT are given in the Supplemental Material. Now it should be obvious that (9) can be rewritten as a strange correlator $Z_M = \langle \Omega | \Psi \rangle$, where $|\Psi\rangle$ is the ground state of the Levin-Wen model corresponding to the fusion category \mathcal{C} . It is well known that such a wave-function on a two dimension surface can be constructed using the Turaev Viro formulation of TQFT path-integral over a triangulated three ball [22]. For a surface triangulation that matches the tiling as specified in (9), the Levin-Wen ground state wavefunction can be written as [22, 27, 28]:

$$|\Psi\rangle = \sum_{\{a_v\}} \sum_{\{i\}} \prod_e d_i^{1/2} \prod_v \omega_a \prod_{\Delta} \left[\begin{array}{ccc} i & j & k \\ c & a & b \end{array} \right] |\{i\}\rangle, \quad (23)$$

The ket $|\{i\}\rangle$ are basis states living on the edges which carries a label $i \in \mathcal{C}$, and

$$\langle \Omega | = \sum_{\{(i,I)\}} \langle \{i\} | \prod_{\Delta} \gamma_{IJK}^{ijk}. \quad (24)$$

The crossing relation (4), together with (48) guarantees that $\langle \Omega |$ is an eigenstate of the RG operator proposed in [24]. We note that the entanglement brane boundary condition (48) follows simply from the prescription of the Turaev-Viro formation of the path-integral. The weights assigned to each internal edge that is summed agrees with the weighted sum of the Cardy states in (48). In other words, the associated 3d TQFT constructed from \mathcal{C} knows about how to close holes in the RCFT.

When constructing non-diagonal RCFTs, the boundary conditions of the CFT correspond to corner variables placed on triangles, which are generally labeled by objects from a "module category" $\mathcal{M}_{\mathcal{C}}$ associated with the fusion category \mathcal{C} . According to the TQFT framework [22], the corner variable should be summed with the weights given by the quantum dimension of the label as an object in the module category. This summation procedure yields the appropriate entanglement brane boundary conditions for general RCFTs. The strange correlator representation of the exact two-dimensional CFT partition function serves as an explicit, practical, and easily computable realization of the holographic relationship between a quantum field theory with categorical symmetry and a TQFT in one higher dimension, as advocated in Ref. [29, 30].

Conclusion and discussion — In conclusion, we present a concrete construction of FP tensors for RCFTs based on the holographic principle. Specifically, the FP tensor can be viewed as a correlation function of RCFT involving "boundary-changing operators" defined on triangles. Our proposed construction of the FP tensor naturally fulfills all the requirements of real space RG conditions. This approach provides a novel avenue for exploring the FP tensor of conformal field theory in higher dimensions, offering exciting possibilities for further investigation.

Despite satisfying all the real-space RG conditions, constructing the conformal map χ for the FP tensor still poses a challenge due to gauge freedom. We address this issue in the Supplemental Material, where we discuss two distinct conformal maps derived using different methodologies. One of these constructions involves a continuous parameter θ , which, when adjusted, has the potential to generate a continuous spectrum of valid FP tensors. While the gauge freedom complicates direct comparisons between our constructed tensor components and those obtained numerically, the successful reproduction of the bulk states spectrum, while satisfying all RG conditions, serves as a robust validation of our approach. Finally, we stress that our constructions can be naturally generalized into higher dimensions, which might allow us to reformulate all CFTs in terms of tensor networks.

Acknowledgments – We acknowledge useful discussions with Yikun Jiang, Bingxin Lao, Nicolai Reshetikhin, Gabriel Wong and Xiangdong Zeng. This work is supported by funding from Hong Kong's Research Grants Council (GRF no.14301219) and Direct Grant no. 4053578 from The Chinese University of Hong Kong. LYH acknowledges the support of NSFC (Grant No. 11922502, 11875111). LC acknowledges the support of NSFC (Grant No. 12305080) and the start up funding of South China University of Technology. GC acknowledges the support from Commonwealth Cyber Initiative at Virginia Tech, U.S. Department of Energy, Office of Science, Office of Advanced Scientific Computing Research.

* These authors contribute equally.

† corresponding to: zcgu@phy.cuhk.edu.hk

‡ corresponding to: lyhung@tsinghua.edu.cn

- [1] G. Vidal, Entanglement renormalization, *Phys. Rev. Lett.* **99**, 220405 (2007).
- [2] Z.-C. Gu, M. Levin, and X.-G. Wen, Tensor-entanglement renormalization group approach as a unified method for symmetry breaking and topological phase transitions, *Phys. Rev. B* **78**, 205116 (2008).
- [3] G. Evenbly and G. Vidal, Algorithms for entanglement renormalization, *Phys. Rev. B* **79**, 144108 (2009).
- [4] R. N. C. Pfeifer, G. Evenbly, and G. Vidal, Entanglement renormalization, scale invariance, and quantum criticality, *Phys. Rev. A* **79**, 040301 (2009).
- [5] Z.-C. Gu and X.-G. Wen, Tensor-entanglement-filtering renormalization approach and symmetry-protected topological order, *Phys. Rev. B* **80**, 155131 (2009).
- [6] M. Levin and C. Nave, Tensor renormalization group approach to two-dimensional classical lattice models, *Phys. rev. Lett.* **99**, 120601 (2007).
- [7] Z.-Y. Xie, H.-C. Jiang, Q.-J. N. Chen, Z.-Y. Weng, and T. Xiang, Second renormalization of tensor-network states, *Phys. rev. Lett.* **103**, 160601 (2009).
- [8] Z. Y. Xie, J. Chen, M. P. Qin, J. W. Zhu, L. P. Yang, and T. Xiang, Coarse-graining renormalization by higher-order singular value decomposition, *Phys. Rev. B* **86**, 045139 (2012).
- [9] G. Evenbly and G. Vidal, Tensor network renormalization, *Phys. rev. Lett.* **115**, 180405 (2015).
- [10] S. Yang, Z.-C. Gu, and X.-G. Wen, Loop optimization for tensor network renormalization, *Phys. rev. Lett.* **118**, 110504 (2017).
- [11] G. Li, K. H. Pai, and Z.-C. Gu, Tensor-network renormalization approach to the q -state clock model, *Phys. Rev. Res.* **4**, 023159 (2022).
- [12] A. Ueda and M. Yamazaki, Fixed-point tensor is a four-point function, (2023), [arXiv:2307.02523 \[cond-mat.stat-mech\]](https://arxiv.org/abs/2307.02523).
- [13] W. Ji and X.-G. Wen, Categorical symmetry and noninvertible anomaly in symmetry-breaking and topological phase transitions, *Phys. Rev. Res.* **2**, 033417 (2020).
- [14] L. Kong, T. Lan, X.-G. Wen, Z.-H. Zhang, and H. Zheng, Algebraic higher symmetry and categorical symmetry: A holographic and entanglement view of symmetry, *Phys. Rev. Res.* **2**, 043086 (2020).

- [15] A. Chatterjee and X.-G. Wen, Holographic theory for continuous phase transitions: Emergence and symmetry protection of gaplessness, *Phys. Rev. B* **108**, 075105 (2023).
- [16] L. Y. Hung and G. Wong, Entanglement branes and factorization in conformal field theory, *Phys. Rev. D* **104**, 026012 (2021), [arXiv:1912.11201 \[hep-th\]](#).
- [17] E. M. Brehm and I. Runkel, Lattice models from CFT on surfaces with holes: I. Torus partition function via two lattice cells, *J. Phys. A* **55**, 235001 (2022), [arXiv:2112.01563 \[cond-mat.stat-mech\]](#).
- [18] R. Vanhove, M. Bal, D. J. Williamson, N. Bultinck, J. Haegeman, and F. Verstraete, Mapping topological to conformal field theories through strange correlators, *Phys. Rev. Lett.* **121**, 177203 (2018).
- [19] D. Aasen, P. Fendley, and R. S. K. Mong, Topological Defects on the Lattice: Dualities and Degeneracies, (2020), [arXiv:2008.08598 \[cond-mat.stat-mech\]](#).
- [20] Y.-Z. You, Z. Bi, A. Rasmussen, K. Slagle, and C. Xu, Wave Function and Strange Correlator of Short Range Entangled states, *Phys. Rev. Lett.* **112**, 247202 (2014), [arXiv:1312.0626 \[cond-mat.str-el\]](#).
- [21] M. A. Levin and X.-G. Wen, String net condensation: A Physical mechanism for topological phases, *Phys. Rev. B* **71**, 045110 (2005), [arXiv:cond-mat/0404617](#).
- [22] V. G. Turaev and O. Y. Viro, State sum invariants of 3 manifolds and quantum 6j symbols, *Topology* **31**, 865 (1992).
- [23] For a physics review of Turaev-Viro models one can consult for example [19].
- [24] L. Chen, H. Zhang, H.-C. Zhang, K.-X. Ji, C. Shen, R.-s. Wang, X.-d. Zeng, and L.-Y. Hung, Exact Holographic Tensor Networks – Constructing CFT_D from TQFT_{D+1}, (2022), [arXiv:2210.12127 \[hep-th\]](#).
- [25] T. Kojita, C. Maccaferri, T. Masuda, and M. Schnabl, Topological defects in open string field theory, *JHEP* **04**, 057, [arXiv:1612.01997 \[hep-th\]](#).
- [26] J. Fuchs, I. Runkel, and C. Schweigert, TFT construction of RCFT correlators IV: Structure constants and correlation functions, *Nucl. Phys. B* **715**, 539 (2005), [arXiv:hep-th/0412290](#).
- [27] Z.-C. Gu, M. Levin, B. Swingle, and X.-G. Wen, Tensor-product representations for string-net condensed states, *Phys. Rev. B* **79**, 085118 (2009).
- [28] O. Buerschaper, M. Aguado, and G. Vidal, Explicit tensor network representation for the ground states of string-net models, *Phys. Rev. B* **79**, 085119 (2009).
- [29] D. Gaiotto and J. Kulp, Orbifold groupoids, *JHEP* **02**, 132, [arXiv:2008.05960 \[hep-th\]](#).
- [30] Y.-H. Lin, M. Okada, S. Seifnashri, and Y. Tachikawa, Asymptotic density of states in 2d CFTs with non-invertible symmetries, *JHEP* **03**, 094, [arXiv:2208.05495 \[hep-th\]](#).

Convention for 6j-symbols and F symbols

The crossing kernels $[F_l^{ijk}]_{mn}$ after being rescaled in the main text, which are often also referred to as the Racah coefficients in the literature, are related to quantum 6j-symbols as follows:

$$F_{mn} \begin{bmatrix} j & k \\ i & l \end{bmatrix} = \sqrt{d_m d_n} \begin{bmatrix} i & j & m \\ k & l & n \end{bmatrix}. \quad (25)$$

The quantum 6j symbols denoted by object in square brackets, enjoy full tetrahedral symmetry. In this gauge it fixes a number of components to:

$$\begin{bmatrix} a & a & 0 \\ b & b & c \end{bmatrix} = \begin{bmatrix} a & b & c \\ b & a & 0 \end{bmatrix} = \frac{N_{ab}^c}{\sqrt{d_a d_b}}. \quad (26)$$

Correspondingly,

$$[F_b^{aab}]_{0c} = \sqrt{\frac{d_c}{d_a d_b}}. \quad (27)$$

As described in the main text, the Racah coefficients are related to the crossing kernels describing crossing relations between canonically normalised conformal blocks by a re-scaling.

For the Ising CFT, the F^{blocks} are given by the expressions below with the parameter $\lambda = 1/2$:

$$F_{11} \begin{bmatrix} \psi & \psi \\ \psi & \psi \end{bmatrix} = 1, \quad (28)$$

$$F_{11} \begin{bmatrix} \sigma & \sigma \\ \sigma & \sigma \end{bmatrix} = -F_{\psi\psi} \begin{bmatrix} \sigma & \sigma \\ \sigma & \sigma \end{bmatrix} = \frac{1}{\sqrt{2}}, \quad (29)$$

$$F_{1\psi} \begin{bmatrix} \sigma & \sigma \\ \sigma & \sigma \end{bmatrix} = \frac{\lambda}{\sqrt{2}}, \quad F_{\psi 1} \begin{bmatrix} \sigma & \sigma \\ \sigma & \sigma \end{bmatrix} = \frac{1}{\sqrt{2}\lambda}, \quad (30)$$

$$F_{1\sigma} \begin{bmatrix} \psi & \sigma \\ \psi & \sigma \end{bmatrix} = F_{1\sigma} \begin{bmatrix} \sigma & \psi \\ \sigma & \psi \end{bmatrix} = \lambda, \quad (31)$$

$$F_{\sigma 1} \begin{bmatrix} \psi & \psi \\ \sigma & \sigma \end{bmatrix} = F_{\sigma 1} \begin{bmatrix} \sigma & \sigma \\ \psi & \psi \end{bmatrix} = \frac{1}{\lambda}, \quad (32)$$

$$F_{\sigma\sigma} \begin{bmatrix} \psi & \sigma \\ \sigma & \psi \end{bmatrix} = F_{\sigma\sigma} \begin{bmatrix} \sigma & \psi \\ \psi & \sigma \end{bmatrix} = -1. \quad (33)$$

The Racah coefficients of the Ising model are given by the same expressions above with $\lambda = 1$. The corresponding 6j symbols are given by

$$\begin{bmatrix} \sigma & \sigma & 1 \\ \sigma & \sigma & 1 \end{bmatrix} = \begin{bmatrix} \sigma & \sigma & 1 \\ \sigma & \sigma & \psi \end{bmatrix} = \frac{1}{\sqrt{2}}, \quad \begin{bmatrix} \sigma & \sigma & \psi \\ \sigma & \sigma & \psi \end{bmatrix} = \frac{-1}{\sqrt{2}}, \quad (34)$$

$$\begin{bmatrix} 1 & 1 & 1 \\ \sigma & \sigma & \sigma \end{bmatrix} = \begin{bmatrix} 1 & \psi & \psi \\ \sigma & \sigma & \sigma \end{bmatrix} = 2^{-\frac{1}{4}}. \quad (35)$$

One can readily check that they are indeed related to F^{blocks} by a rescaling of the form

$$[F_l^{ijk}]_{mn} = [F_l^{ijk}]_{mn}^{\text{blocks}} \frac{\mathcal{N}_{jkn} \mathcal{N}_{inl}}{\mathcal{N}_{ijm} \mathcal{N}_{mkl}}. \quad (36)$$

Conformal maps defining the fixed point tensor

In this section we explicitly evaluate the tensor defined as path integral on Riemann surface with boundaries, as shown in Fig. 5a. To achieve this we construct a conformal transformation χ to map this region to upper-half-plane, and shrink the three boundary states to local operators inserted on the real axis (Fig. 5b).



FIG. 5: Conformal transformation that maps triangular region to upper-half-plane with three local operators inserted on the real-axis.

In the following, we present two distinct approaches for constructing the map. The first approach leverages the state-operator correspondence principle. The second approach takes a different route by treating the triangular region as an amputated pants-diagram.

Method I: state-operator correspondence.— The state-operator correspondence is implemented through a map f from the Upper-Half-Plane (UHP) to a designated segment region, as shown in Fig. 6a. Through this map we prepare the state $|O_i^{ab}\rangle$ by inserting operator O_i^{ab} at origin.

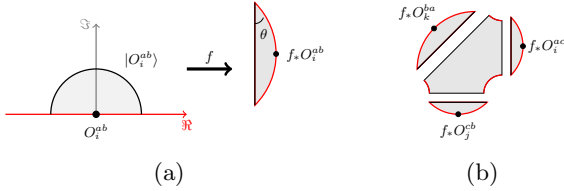


FIG. 6: (a) A single segment region is mapped to upper-half-plane through a function f . (b) The triangular region attaches three segment regions along the open boundaries.

Then we apply these prepared states to the three open boundaries of the triangular region, Fig. 5a. Diagrammatically, this process is represented by attaching the segments along the three open boundaries as shown in Fig. 6b.

We further require that the prepared states form an orthonormal basis in the Hilbert space of boundary CFT. The inner product of these states is determined by the two-point function, which is evaluated over the double-segment region as shown in Fig. 7. The condition of

orthonormality is expressed through the following relationship:

$$\langle f_*[O_j(0)^\dagger] f_*[O_i(0)] \rangle_{\text{double-segment}} = \delta_{ij}. \quad (37)$$

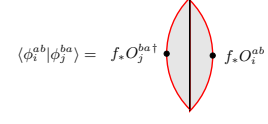


FIG. 7: The double segment region obtained by gluing two segments regions.

The conformal map f satisfying this condition is given by the following complicate composite function:

$$f(z) = \xi \circ \eta \circ \omega(z) \\ \omega(z) = \frac{1+z}{1-z}, \quad \eta(\omega) = e^{-i\theta} \omega^{\frac{2\theta}{\pi}}, \quad \xi(\eta) = i \frac{\eta-1}{\eta+1}. \quad (38)$$

Here we have a free parameter θ which is the angle of the corner in the segment region (see Fig. 6a). This angle serves as a gauge freedom of our tensor construction. For computation simplicity we choose to set $\theta = \frac{\pi}{4}$.

Following this, we proceed by shrinking the corners of the triangular region (refer to Fig. 5a) to zero length. This leads to the derivation of the tensor, now represented as a three-point function on the area shown in Fig. 8a.



FIG. 8: Conformal transformation that maps triangular shaped disk to upper-half-plane

In the final step we find a function $g(\xi)$ that maps the disk (Fig. 8a) to the UHP (Fig. 8b). Given the gauge choice $\theta = \frac{\pi}{4}$, we write down the function $g(\xi)$ explicitly as,

$$g(\xi) = \left(-i \frac{\xi + (1+i)}{\xi - (1+i)}\right)^{\frac{4}{3}}. \quad (39)$$

After applying the conformal transformation $g(\xi)$, The operators on upper-half-plane Fig. 8b becomes $\chi_{1*} O_i^{ac}(0)$, $\chi_{2*} O_j^{cb}(0)$ and $\chi_{3*} O_k^{ba}(0)$. So the tensor components are equal to the following three point function on upper-half-plane,

$$\alpha_{IJK}^{ijk} = \langle \chi_{1*} O_{(I,i)}(0) \chi_{2*} O_{(J,j)}(0) \chi_{3*} O_{(K,k)}(0) \rangle_{UHP}, \quad (40)$$

where the χ -functions are defined as,

$$\begin{aligned}\chi_1(z) &= g(f(z) + 1), \quad \chi_2(z) = g(-if(z) - i), \\ \chi_3(z) &= g(\sqrt{2}e^{i\frac{3\pi}{4}}f(z)).\end{aligned}\quad (41)$$

As a simple example, consider the three operators all primary fields with bulk conformal dimension being Δ_1 , Δ_2 and Δ_3 . Then the tensor component are calculated as,

$$\alpha_{000}^{\Delta_1\Delta_2\Delta_3} \approx 0.515^{\Delta_1+\Delta_2} 0.839^{\Delta_3}. \quad (42)$$

Method II: Pants-diagram— The second strategy we present here is to treat the triangular region as an amputated pants-diagram, as shown in Fig. 9. The function χ is a map from this pants-diagram to UHP.

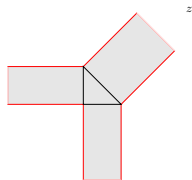


FIG. 9: pants-diagram

First we adopt the Schwarz–Christoffel transformation to find the map from upper-half-plane to the pants-diagram,

$$h(\xi) = \int^\xi dx \frac{\sqrt{2}(5x^2 - 1)^{\frac{1}{4}}}{x(x^2 - 1)}. \quad (43)$$

This function maps the three points -1 , 0 and 1 of the UHP to three infinities along the legs of pants, where we attach free open string states. Near these infinities, we have the following expansions:

$$\begin{aligned}h|_{\xi \rightarrow 1} &\sim \ln|\xi - 1|, \quad h|_{\xi \rightarrow 0} \sim -(1+i)\ln|\xi| + i\pi, \\ h|_{\xi \rightarrow -1} &\sim i\ln|\xi + 1| + \pi.\end{aligned}\quad (44)$$

These are precisely the functions we can utilize to prepare open string states at infinities. According to these relations, we define the conformal functions,

$$\begin{aligned}\chi_1(z) &:= h^{-1}(\ln z), \quad \chi_2(z) := h^{-1}(i\ln z + \pi), \\ \chi_3(z) &:= h^{-1}(-(1+i)\ln z + i\pi).\end{aligned}\quad (45)$$

It's hard to find a concise expression for the inverse function of the map $h(\xi)$. Instead, we expand this function around the singularities as,

$$\begin{aligned}\chi_1(z) &= 1 + 0.9z + 0.709z^2 + 0.641z^3 + O(z^4) \\ \chi_2(z) &= -1 + 0.9z - 0.709z^2 + 0.641z^3 + O(z^4) \\ \chi_3(z) &= 0.410z + 0.008z^3 + O(z^5)\end{aligned}\quad (46)$$

This allows us to evaluate the tensor numerically. Again, we present the tensor component for primary fields,

$$\alpha_{000}^{\Delta_1\Delta_2\Delta_3} \approx 0.671^{\Delta_1+\Delta_2} 0.905^{\Delta_3}. \quad (47)$$

Proof of RG equations— The construction in both approaches guarantee the equivalence between contracting the tensors and gluing the Riemann surfaces. The crossing symmetry condition follows directly from this property.

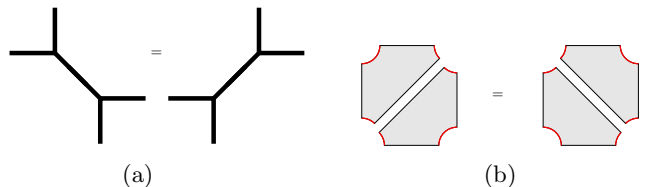


FIG. 10: (a) Two ways of contracting rank-3 tensors are equivalent. (b) Two ways of gluing triangular-shaped Riemann surfaces are equivalent.

We can also prove the other properties diagrammatically. Fig. 11 shows proof of the fixed point tensor property. The rank-4 tensor in Fig. 11a is obtained by contracting four rank-3 tensors. This corresponds to the square-shaped region in Fig. 11b. The hole in the center of this region is shrunk to zero dimension and projected to ground state due to long Euclidean time evolution and the closing condition (48).

$$\sum_i \omega_i |i\rangle_c = |0\rangle, \quad (48)$$

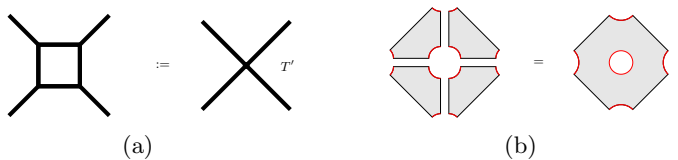


FIG. 11: (a) Contraction of four tensors in a loop. (b) Gluing four triangles to a single Riemann surface.

Finally, Fig. 12 illustrates the process of self-contraction to obtain the partition function on torus. The contraction of opposite legs corresponds to fusion of opposing edges of the square-shaped region, as depicted in Fig. 12b. The outcome of this procedure is a path integral on a torus defected by a central hole. Again, the boundary state residing on this small hole can be projected to the ground state as the dimension of the hole is reduced to zero.

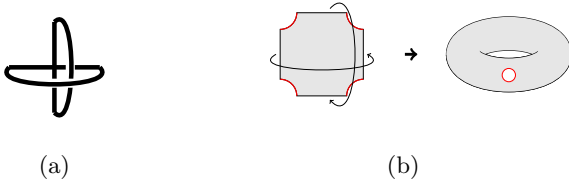


FIG. 12: Contraction the opposite legs of fixed point tensor produces partition function on torus.

To obtain the closed string spectrum, we tiling multiple tensors into a cylinder, as shown in Fig. 13. This can be viewed as a transfer matrix M_{IJ} , where I, J are collections of both the descendant indices and boundary condition indices, namely $I = \{i_1, i_2, \dots, i_n, a_1, a_2, \dots, a_n\}$ and $J = \{j_1, j_2, \dots, j_n, b_1, b_2, \dots, b_n\}$. Here, n represents the number of rank-4 tensors used in the tiling process. Hence the reciprocal of n is equal to moduli of the cylinder. Consequently, the reciprocal of n determines the moduli of the cylinder. Diagonalizing this transfer matrix yields the desired spectrum of CFT bulk states, expressed as:

$$\lambda_i = C e^{\frac{2\pi}{n} \Delta_i} \quad (49)$$

where C is a constant depends on normalization of the tensor. In the following, we provide the spectrum data calculated from various cylinder moduli and bond dimensions in Table II, III, IV. Each column in these tables is labeled according to the cutoff in descendant levels for the fields on the three tensor legs. The data clearly demonstrate a consistent convergence of the computed conformal dimension towards the precise value as the cutoff increases.

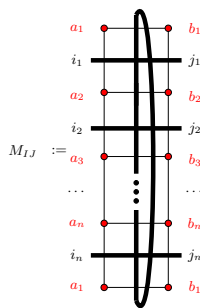


FIG. 13: The transfer matrix

State/Cutoff	007	117	227	337	447	exact
$\mathbb{1}$	0.0000	0.0000	0.0000	0.0000	0.0000	0.0000
σ	0.1245	0.1249	0.1249	0.1250	0.1250	0.1250
ϵ	1.0293	1.0029	0.9930	0.9963	0.9989	1.0000
$\partial\sigma, \bar{\partial}\sigma$	1.1708	1.1324	1.1255	1.1237	1.1253	1.1250
$\partial\epsilon, \bar{\partial}\epsilon$	2.1345	2.0196	2.0030	2.0004	1.9985	2.0000
$\mathbb{1}^{(-2)}, \bar{\mathbb{1}}^{(-2)}$	2.2234	2.0301	1.9859	1.9899	1.9986	2.0000
$\partial\bar{\partial}\sigma$	2.3037	2.1449	2.1227	2.1045	2.1099	2.1250
$\sigma^{(-2)}, \bar{\sigma}^{(-2)}$	2.5273	2.1591	2.1330	2.1086	2.1208	2.1250
$\partial\bar{\partial}\epsilon$	3.0715	3.0345	2.9904	2.9384	2.9517	3.0000
$\partial^2\epsilon, \bar{\partial}^2\epsilon$	2.9115	3.0568	2.9732	2.9929	3.0030	3.0000
$\mathbb{1}^{(-3)}, \bar{\mathbb{1}}^{(-3)}$	2.9839	3.0491	2.9849	2.9333	2.9496	3.0000
$\bar{\partial}\sigma^{(-2)}, \partial\bar{\sigma}^{(-2)}$	3.0689	3.1085	3.0083	2.9444	2.9900	3.1250
$\partial\sigma^{(-2)}, \bar{\partial}\bar{\sigma}^{(-2)}$	3.6670	3.1805	3.0902	3.1065	3.1167	3.1250
$\sigma^{(-3)}, \bar{\sigma}^{(-3)}$	3.6973	3.2351	3.1346	3.1085	3.1291	3.1250
$\mathbb{1}^{(-2,-2)}$	4.0464	4.0442	4.0446	4.0431	4.0323	4.0000

TABLE II: Data from cylinder with length $n = 4$. Columns are labeled by the cutoff in descendant levels of the three legs of tensor. The actual bond dimensions correspond to the number of fields up to the specified descendant level cutoff. For instance, the bond dimensions for a cutoff of 447 is (7,7,22).

State/Cutoff	007	117	227	337	447	exact
$\mathbb{1}$	0.0000	0.0000	0.0000	0.0000	0.0000	0.0000
σ	0.1241	0.1248	0.1249	0.1250	0.1250	0.1250
ϵ	1.0541	1.0051	0.9878	0.9935	0.9980	1.0000
$\partial\sigma, \bar{\partial}\sigma$	1.2115	1.1380	1.1258	1.1226	1.1253	1.1250
$\partial\epsilon, \bar{\partial}\epsilon$	2.1398	2.0356	1.9798	1.9873	1.9924	2.0000
$\mathbb{1}^{(-2)}, \bar{\mathbb{1}}^{(-2)}$	2.2034	2.0554	2.0090	1.9902	2.0038	2.0000
$\partial\bar{\partial}\sigma$	2.2050	2.1618	2.0870	2.1022	2.1204	2.1250
$\sigma^{(-2)}$	2.3574	2.1582	2.0954	2.0576	2.0737	2.1250

TABLE III: Data from cylinder with length $n = 3$.

State/Cutoff	007	117	227	337	447	exact
$\mathbb{1}$	0.0000	0.0000	0.0000	0.0000	0.0000	0.0000
σ	0.1231	0.1247	0.1246	0.1250	0.1250	0.1250
ϵ	1.1146	0.9751	1.0110	0.9862	0.9955	1.0000
$\partial\sigma, \bar{\partial}\sigma$	1.3039	1.1313	1.1401	1.1166	1.1232	1.1250

TABLE IV: Data from cylinder with length $n = 2$.

Iteration relations

Transformation rules — In this section, we present details in mapping descendant fields under a conformal transformation $\chi(z)$. For more general descendant fields, we can not give a simple expression for the transformation coefficients, but deriving an iteration relation is possible.

Suppose that we already know the transformation rule for the operator $O^{(-k_l, \dots, -k_2, -k_1)} := L_{-k_l} \cdots L_{-k_2} L_{-k_1} O$. The transformation under holomorphic function $\chi(z)$ is written as

$$\chi_* O^{(-k_l, \dots, -k_2, -k_1)}(z) = \sum_{\{k'\} \leq \{k\}} H_{k'_l, \dots, k'_2, k'_1}^{k_l, \dots, k_2, k_1}(z) O^{(-k'_l, \dots, -k'_2, -k'_1)}(\eta), \quad (50)$$

where $\eta = \chi(z)$, and the symbol $\{k\}$ is a shorthand notation of $\{k_l, \dots, k_2, k_1\}$. $\{k'\} \leq \{k\}$ means that $\forall k_i \in \{k\}$, $k'_i \leq k_i$. Moreover, suppose that we also know the OPE between $T(z)$ and $O^{(-k_l, \dots, -k_2, -k_1)}(z')$:

$$\begin{aligned} T(z) O^{(-k_l, \dots, -k_2, -k_1)}(z') &= \sum_{k'_{l+1}} (z - z')^{k'_{l+1} - 2} O^{(-k'_{l+1}, -k_l, \dots, -k_2, -k_1)}(z') \\ &+ \sum_{\{k'\} \leq \{k\}} \frac{C_{k'_l, \dots, k'_2, k'_1}^{k_l, \dots, k_2, k_1}}{(z - z')^{\sum_{p=1}^l k_p - \sum_{p=1}^l k'_p + 2}} O^{(-k'_l, \dots, -k'_2, -k'_1)}(z'). \end{aligned} \quad (51)$$

Then we can derive the transformation rule for higher level descendant field $O^{(-k_{l+1}, -k_l, \dots, -k_2, -k_1)}$ as

$$\begin{aligned} &\chi_* O^{(-k_{l+1}, -k_l, \dots, -k_2, -k_1)}(z') \\ &= \oint_{z'} \frac{dz}{2\pi i} (z - z')^{1 - k_{l+1}} \chi_* T(z) \chi_* O^{(-k_l, \dots, -k_2, -k_1)}(z') \\ &= \oint_{\eta'} \frac{d\eta}{2\pi i} \frac{(z - z')^{1 - k_{l+1}}}{\chi'(z)} [\chi'(z)^2 T(\eta) + \frac{c}{12} \{\chi(z), z\}] \sum_{\{k'\} \leq \{k\}} H_{k'_l, \dots, k'_2, k'_1}^{k_l, \dots, k_2, k_1}(z') O^{(-k'_l, \dots, -k'_2, -k'_1)}(\eta') \\ &= \sum_{\{k'\} \leq \{k\}} \sum_{k'_{l+1}=0}^{k_{l+1}} H_{k'_l, \dots, k'_2, k'_1}^{k_l, \dots, k_2, k_1}(z') a_{k_{l+1} - k'_{l+1}}^{k_{l+1}}(z') O^{(-k'_{l+1}, -k'_l, \dots, -k'_2, -k'_1)}(\eta') \\ &+ \sum_{\{k''\} \leq \{k\}} \left[\sum_{\{k'\} \leq \{k'\} \leq \{k\}} H_{k'_l, \dots, k'_2, k'_1}^{k_l, \dots, k_2, k_1}(z') a_{k_{l+1} + \sum k'' - \sum k'}^{k_{l+1}}(z') C_{k''_l, \dots, k''_2, k''_1}^{k'_l, \dots, k'_2, k'_1} \right] O^{(-k''_l, \dots, -k''_2, -k''_1)}(\eta') \\ &+ \frac{c}{12(k_{l+1} - 2)!} \left(\frac{d}{dz} \right)^{k_{l+1} - 2} \{\chi(z), z\} \Big|_{z=z'} \sum_{\{k'\} \leq \{k\}} H_{k'_l, \dots, k'_2, k'_1}^{k_l, \dots, k_2, k_1}(z') O^{(-k'_l, \dots, -k'_2, -k'_1)}(\eta'), \end{aligned} \quad (52)$$

where the coefficients a_m^n 's are defined by

$$\chi'(z)(z - z')^{1-n} = (\eta - \eta')^{1-n} \sum_{m=0}^{\infty} a_m^n(z') (\eta - \eta')^m. \quad (53)$$

Comparing with the definition of these transformation coefficients we conclude that,

$$\begin{aligned} H_{k'_{l+1}, k'_l, \dots, k'_2, k'_1}^{k_{l+1}, k_l, \dots, k_2, k_1}(z') &= H_{k'_l, \dots, k'_2, k'_1}^{k_l, \dots, k_2, k_1}(z') a_{k_{l+1} - k'_{l+1}}^{k_{l+1}}(z') \\ H_{k'_{l+1}, k_l, \dots, k'_2, k'_1}^{k_{l+1}, k_l, \dots, k_2, k_1}(z') &= \sum_{\{k'\} \leq \{k'\} \leq \{k\}} a_{k_{l+1} + \sum k'' - \sum k'}^{k_{l+1}}(z') H_{k'_l, \dots, k'_2, k'_1}^{k_l, \dots, k_2, k_1}(z') C_{k''_l, \dots, k''_2, k''_1}^{k'_l, \dots, k'_2, k'_1} \\ &+ \frac{c}{12(k_{l+1} - 2)!} \left(\frac{d}{dz} \right)^{k_{l+1} - 2} \{\chi(z), z\} \Big|_{z=z'} H_{k'_l, \dots, k'_2, k'_1}^{k_l, \dots, k_2, k_1}(z'). \end{aligned} \quad (54)$$

OPE coefficients — Now we derive an iteration relation of the OPE coefficient between energy momentum tensor $T(z)$ and a general descendant field $O^{(-k_l, \dots, -k_2, -k_1)}(z')$. The OPE coefficients are denoted by the symbol $C_{k'_l, \dots, k'_2, k'_1}^{k_l, \dots, k_2, k_1}$

defined as,

$$\begin{aligned}
T(z)O^{(-k_l, \dots, -k_2, -k_1)}(z') &= \sum_{k'_{l+1}=1}^{\infty} (z-z')^{k'_{l+1}-2} O^{(-k'_{l+1}, -k_l, \dots, -k_2, -k_1)}(z') \\
&+ \sum_{\{k'\} \leq \{k\}} \frac{C_{k'_l, \dots, k'_2, k'_1}^{k_l, \dots, k_2, k_1}}{(z-z')^{\sum_{p=1}^l k_p - \sum_{p=1}^l k'_p + 2}} O^{(-k'_l, \dots, -k'_2, -k'_1)}(z').
\end{aligned} \tag{55}$$

Again, we use the symbol $\{k\}$ to denote the set $\{k_l, \dots, k_2, k_1\}$. $\{k'\} \leq \{k\}$ means that $k'_p \leq k_p$ for any $1 \leq p \leq l$. For the higher level descendants $O^{(-k_{l+1}, -k_l, \dots, -k_2, -k_1)}$, its operator product with $T(z)$ is,

$$\begin{aligned}
&T(z)O^{(-k_{l+1}, -k_l, \dots, -k_2, -k_1)}(z') \\
&= \oint_{z'} \frac{dw}{2\pi i} (w-z')^{1-k_{l+1}} T(z)T(w)O^{(-k_l, \dots, -k_2, -k_1)}(z') \\
&= - \left[\oint_z \frac{dw}{2\pi i} (w-z')^{1-k_{l+1}} T(w)T(z) \right] O^{(-k_l, \dots, -k_2, -k_1)}(z') + \oint_{z'} \frac{dw}{2\pi i} (w-z')^{1-k_{l+1}} T(w) [T(z)O^{(-k_l, \dots, -k_2, -k_1)}(z')] \\
&= \sum_{k'_{l+1}=1}^{k_{l+1}} (2k_{l+1} - k'_{l+1}) \frac{O^{(-k'_{l+1}, -k_l, \dots, -k_2, -k_1)}}{(z-z')^{k_{l+1}-k'_{l+1}+2}} + \sum_{\{k'\} \leq \{k\}} C_{k'_l, \dots, k'_2, k'_1}^{k_l, \dots, k_2, k_1} \frac{O^{(-k_{l+1}, -k'_l, \dots, -k'_2, -k'_1)}(z')}{(z-z')^{\sum_{p=1}^l k_p - \sum_{p=1}^l k'_p + 2}} \\
&+ \sum_{\{k'\} \leq \{k\}} (2k_{l+1} + \sum_{p=1}^l k_p - \sum_{p=1}^l k'_p) C_{k'_l, \dots, k'_2, k'_1}^{k_l, \dots, k_2, k_1} \frac{O^{(-k'_l, \dots, -k'_2, -k'_1)}(z')}{(z-z')^{k_{l+1} + \sum_{p=1}^l k_p - \sum_{p=1}^l k'_p + 2}} \\
&+ \frac{c}{12} k_{l+1} (k_{l+1}^2 - 1) \frac{O^{(-k_l, \dots, -k_2, -k_1)}}{(z-z')^{k_{l+1}+2}} + \dots
\end{aligned} \tag{56}$$

where the ellipsis denotes any combination of descendant operators at level higher than $\sum_{p=1}^{l+1} k_p$. We neglected them simply because we already know their coefficients.

Comparing with the definition of $C_{k'_{l+1}, k'_l, \dots, k'_2, k'_1}^{k_{l+1}, k_l, \dots, k_2, k_1}$, we conclude that,

$$\begin{aligned}
C_{k'_{l+1}, k'_l, \dots, k'_2, k'_1}^{k_{l+1}, k_l, \dots, k_2, k_1} &= 2k_{l+1} - k'_{l+1}, \quad \text{for } 1 \leq k'_{l+1} < k_{l+1} \\
C_{k_{l+1}, k'_l, \dots, k'_2, k'_1}^{k_{l+1}, k_l, \dots, k_2, k_1} &= C_{k'_l, \dots, k'_2, k'_1}^{k_l, \dots, k_2, k_1}, \quad \text{for } \{k'\} < \{k\} \\
C_{k_{l+1}, k_l, \dots, k_2, k_1}^{k_{l+1}, k_l, \dots, k_2, k_1} &= k_{l+1} + C_{k_l, \dots, k_2, k_1}^{k_l, \dots, k_2, k_1} \\
C_{k'_l, \dots, k'_2, k'_1}^{k_{l+1}, k_l, \dots, k_2, k_1} &= (2k_{l+1} + \sum_{p=1}^l k_p - \sum_{p=1}^l k'_p) C_{k'_l, \dots, k'_2, k'_1}^{k_l, \dots, k_2, k_1} + \frac{c}{12} k_{l+1} (k_{l+1}^2 - 1) \delta_{\{k'\}}^{\{k\}}
\end{aligned} \tag{57}$$

Correlation function — We can also derive an iteration equation of correlators. Suppose that we already know all the correlators of lower level descendants, we can derive the higher level ones using this equation.

To simplify the notation, we use $O^{(-\vec{k})}$ to denote $O^{(-k_l, \dots, -k_2, -k_1)}$, and the OPE coefficient $C_{\vec{k}'}^{\vec{k}}$ to denote $C_{k'_l, \dots, k'_2, k'_1}^{k_l, \dots, k_2, k_1}$.

Then we will show that the correlator $\langle L_{-m} O_1^{(-\vec{k})}(x) O_2^{(-\vec{p})}(y) O_3^{(-\vec{q})}(z) \rangle$ can be written as a linear combination of simpler correlators of the form $\langle O_1^{(-\vec{k}')} (x) O_2^{(-\vec{p}')} (y) O_3^{(-\vec{q}')} (z) \rangle$, with $\vec{k}' \leq \vec{k}$, $\vec{p}' \leq \vec{p}$ and $\vec{q}' \leq \vec{q}$ (in the sense of $\{k'\} \leq \{k\}$ defined in the previous sections). We start from the equation,

$$\begin{aligned}
&\langle L_{-m} O_1^{(-\vec{k})}(x) O_2^{(-\vec{p})}(y) O_3^{(-\vec{q})}(z) \rangle \\
&= \oint_x \frac{dw}{2\pi i} (w-x)^{1-m} \langle [T(w)O_1^{(-\vec{k})}(x)] O_2^{(-\vec{p})}(y) O_3^{(-\vec{q})}(z) \rangle \\
&= - \oint_y \frac{dw}{2\pi i} (w-x)^{1-m} \langle O_1^{(-\vec{k})}(x) [T(w)O_2^{(-\vec{p})}(y)] O_3^{(-\vec{q})}(z) \rangle - \oint_z \frac{dw}{2\pi i} (w-x)^{1-m} \langle O_1^{(-\vec{k})}(x) O_2^{(-\vec{p})}(y) [T(w)O_3^{(-\vec{q})}(z)] \rangle
\end{aligned} \tag{58}$$

Using the OPE,

$$T(w)O^{(-\vec{p})}(y) = \sum_{\vec{p}' \leq \vec{p}} C_{\vec{p}'}^{\vec{p}} \frac{O^{(-\vec{p}')} (y)}{(w-y)^{|\vec{p}|-|\vec{p}'|+2}} + \frac{\partial O^{(-\vec{p})}(y)}{w-y} + reg., \quad (59)$$

where *reg.* means the regular terms in the limit $w \rightarrow y$, we can expand the expression,

$$\begin{aligned} & \oint_y \frac{dw}{2\pi i} (w-x)^{1-m} \langle O_1^{(-\vec{k})}(x) [T(w)O_2^{(-\vec{p})}(y)] O_3^{(-\vec{q})}(z) \rangle \\ &= \frac{\partial_y}{(y-x)^{m-1}} \langle O_1^{(-\vec{k})}(x) O_2^{(-\vec{p})}(y) O_3^{(-\vec{q})}(z) \rangle \\ &+ (-1)^{|\vec{p}|-|\vec{p}'|-1} \sum_{\vec{p}' \leq \vec{p}} \frac{C_{\vec{p}'}^{\vec{p}}}{(y-x)^{m+|\vec{p}|-|\vec{p}'|}} \frac{(|\vec{p}|-|\vec{p}'|+m-1)!}{(|\vec{p}|-|\vec{p}'|+1)!(m-2)!} \langle O_1^{(-\vec{k})}(x) O_2^{(-\vec{p}')} (y) O_3^{(-\vec{q})}(z) \rangle. \end{aligned} \quad (60)$$

The other term is calculated similarly. So the correlator is reduced to combinations of simpler ones:

$$\begin{aligned} & \langle L_{-m} O_1^{(-\vec{k})}(x) O_2^{(-\vec{p})}(y) O_3^{(-\vec{q})}(z) \rangle \\ &= - \frac{\partial_y}{(y-x)^{m-1}} \langle O_1^{(-\vec{k})}(x) O_2^{(-\vec{p})}(y) O_3^{(-\vec{q})}(z) \rangle \\ &+ (-1)^{|\vec{p}|-|\vec{p}'|} \sum_{\vec{p}' \leq \vec{p}} \frac{C_{\vec{p}'}^{\vec{p}}}{(y-x)^{m+|\vec{p}|-|\vec{p}'|}} \frac{(|\vec{p}|-|\vec{p}'|+m-1)!}{(|\vec{p}|-|\vec{p}'|+1)!(m-2)!} \langle O_1^{(-\vec{k})}(x) O_2^{(-\vec{p}')} (y) O_3^{(-\vec{q})}(z) \rangle \\ &+ (y \rightarrow z, \vec{p} \rightarrow \vec{q}). \end{aligned} \quad (61)$$